Electronic Supplementary Material (ESI) for Lab on a Chip.

Recognition-Mediated Particle Detection Under Microfluidic Flow with Waveguide-Coupled 2D Photonic Crystals: Towards Integrated Photonic Virus Detectors

J. E. Baker, R. Sriram and B .L. Miller

Supplementary Information

S1. Large-hole defect position

The strength of optical coupling between the point-like large-hole PhC defect and the W1 waveguide is roughly controlled by the number of rows of PhC lattice holes separating the two features. To gain some information about how this affects the transmission dip, 3D FDTD simulations were performed for geometries with three different large-hole defect positions. Cross-sectional representations of the simulated geometries and the resulting spectra are shown in Figure S1. As additional rows of lattice holes were added between the large-defect hole and the W1 waveguide, the depth of the transmission dip was reduced. This was expected, given the photonic band properties of the PhC lattice. The depth of the transmission dip for the case in which the large-defect was centered 6 rows away from the W1 waveguide appeared insufficient for our experimental purposes, but both the other cases remained eligible for fabrication and experiment. The case in which the large-hole defect was centered 3 rows from the W1 waveguide (not shown) produced a dip in resonance with a width exceeding 10 nm, and was also ruled impractical for our experimental purposes.

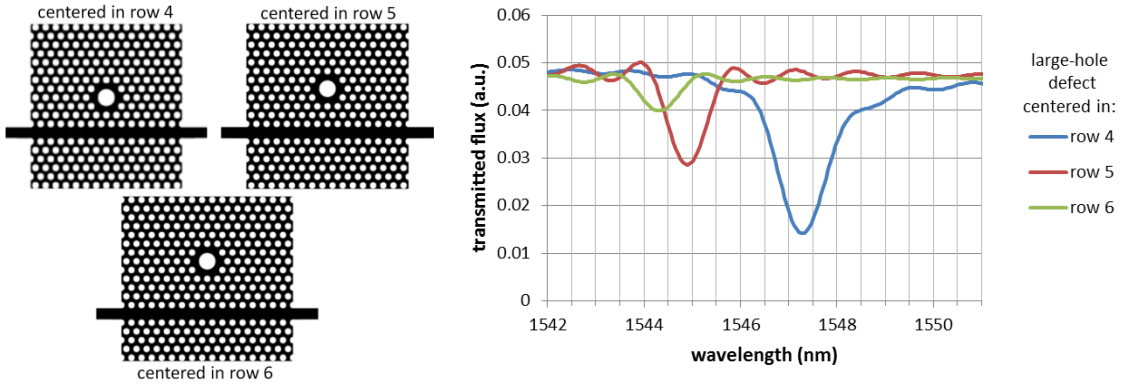

Figure S1. Simulated with 3D FDTD methods, the dip regions of the transmission spectra are plotted for PhC geometries in which the large-hole defect is centered 4, 5, and 6 rows away from the W1 waveguide.

S2. Temperature sensitivity calculation

According to perturbation theory, the fractional change in the frequency of an optical mode of a PhC resonator depends linearly on both the fractional change in refractive index and the fractional portion of electric-field energy in the region where the refractive index is perturbed[1]:

$$\frac{\Delta\omega}{\omega} \cong -\frac{1}{2}\frac{\int d^3\mathrm{r}\,\Delta\varepsilon(\mathrm{r})|\mathrm{E}(\mathrm{r})|^2}{\int d^3\mathrm{r}\,\varepsilon(\mathrm{r})|\mathrm{E}(\mathrm{r})|^2} \cong -\frac{\Delta n}{n}\cdot\left(\text{fraction of}\int \varepsilon|\mathrm{E}|^2 \text{ in perturbed region}\right). \qquad (1)$$

Presuming that the electromagnetic profile does not change significantly, the change in resonance wavelength can be further approximated as:

$$\frac{\Delta\lambda}{\lambda} \cong -\frac{\Delta\omega}{\omega} \cong \frac{\Delta n}{n} \cong \frac{\partial \mathrm{n}}{\partial \mathrm{T}}\,\Delta T, \tag{2}$$

thus yielding a temperature dependence of

$$\frac{\Delta\lambda}{\Delta T} \cong \frac{\lambda}{n}\frac{\partial \mathrm{n}}{\partial \mathrm{T}} = \frac{(1550\ \mathrm{nm})}{3.48}(1.86\times10^{-4}\ \mathrm{K}^{-1}) = 0.083\ \mathrm{nm}\cdot\mathrm{K}^{-1} \tag{3}$$

for the resonance wavelength in a silicon[2] PhC resonator.

S3. Temperature-controlled microfluidic clamp assembly

The clamp assembly design shown in Figure S2 was implemented in order to seal the microfluidic channel-embedded PDMS elastomer over the silicon PhC chip. The clamp also contained a thermo-electric cooling module to maintain constant temperature while measuring optical spectra. The large recess in the side of the cold plate was present to permit adequate room for tapered optical fibers to be aligned with waveguide facets on the side edges of the PhC chip.

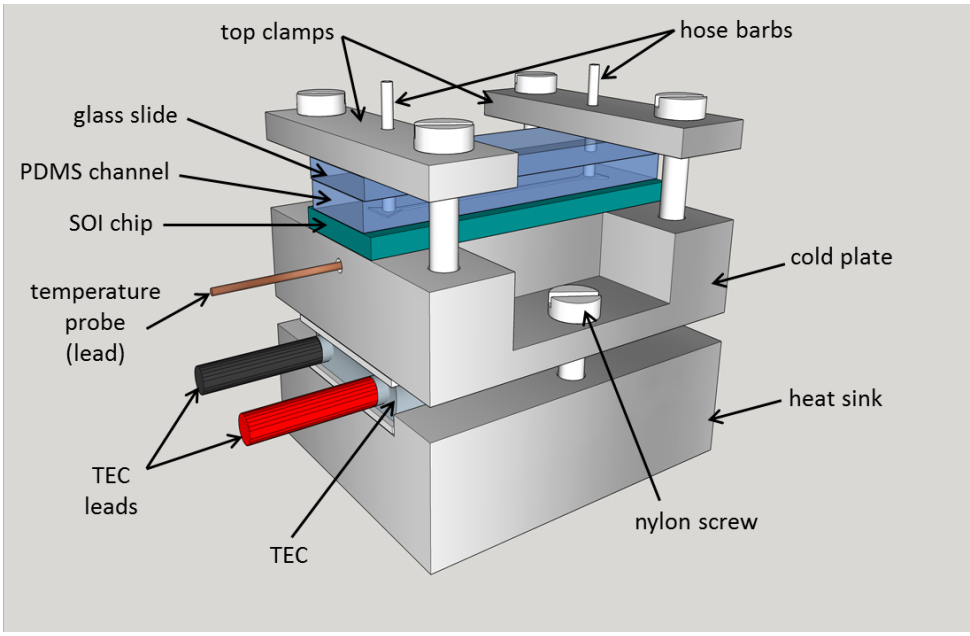

Figure S2. Schematic representation of temperature controlled microfluidic channel clamp assembly, with individual components labeled.

S4. Confirmation of biomolecule activity

The selectivity of the attachment between human-IgG-coated latex microspheres and the anti-human IgG layer on the surface was assayed on flat SiO_2/Si chips. The fluorescence microscopy images shown in Figure S3 demonstrate that microsphere attachment was only frequent when the conjugate immunotarget was attached to the chip surface.

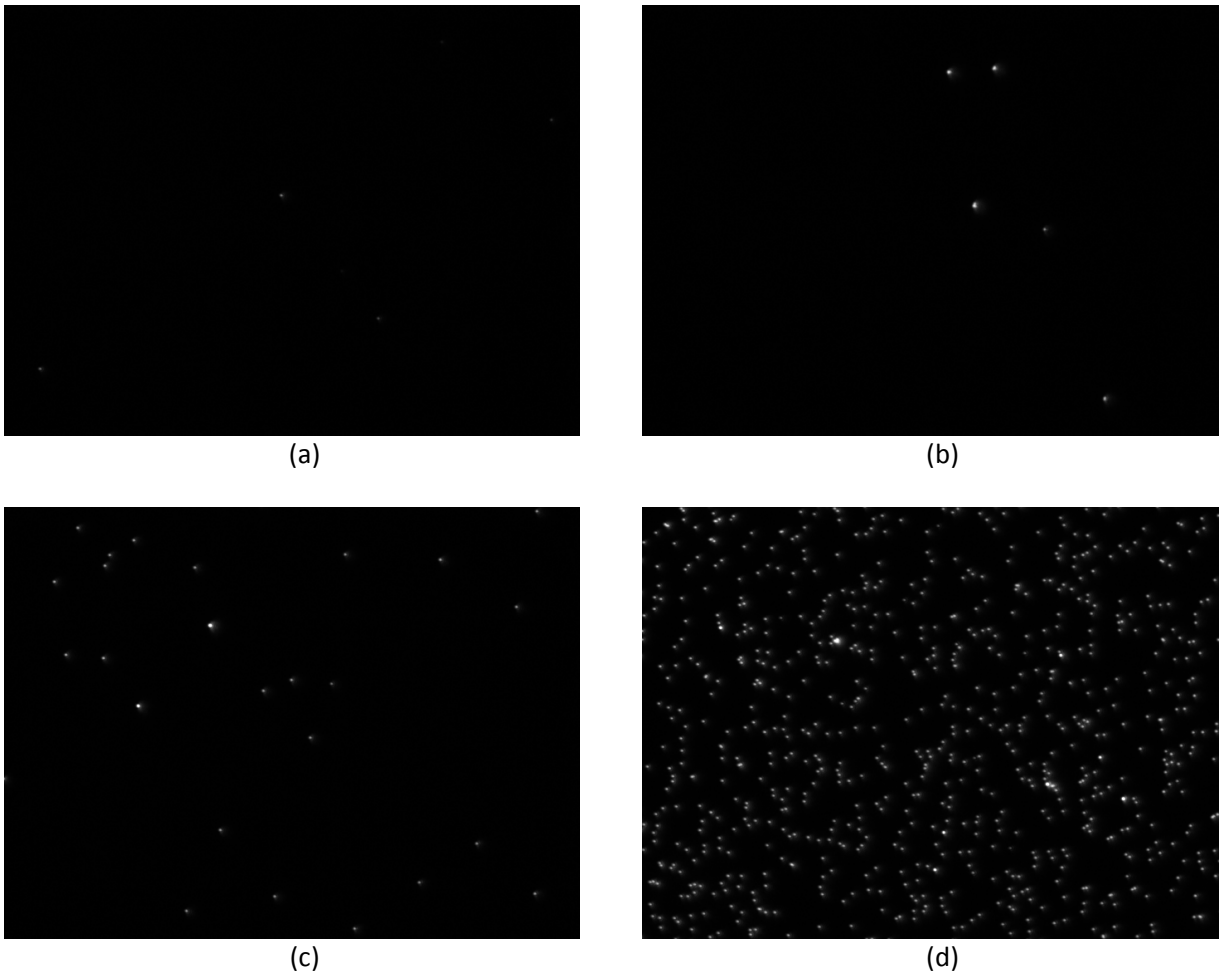

Figure S3: Representative optical microscopy images of the Si/SiO_2 chip incubated with 1:100 dilution of human IgG-modified fluorescent latex particle solution along the different steps of surface functionalization. (a) Piranha cleaned chip surface, (b) silane (APDMES) and glutaraldehyde modified surface, (c) silane and glutaralehyde modified chip subsequently blocked with BSA, and (d) silane/GA modified chip functionalized with goat anti-human IgG. All images are at the same exposure.

S5. Ellipsometric measurement of functionalization layers

To verify attachment of surface chemistry and biochemistry functionalization layers on the PhC sensor, spectroscopic ellipsometry measurements were taken on flat regions of the PhC sensor chip. Results are shown in Figure S4.

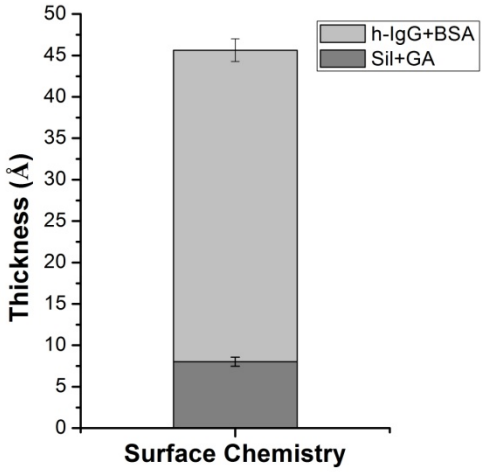

Figure S4: Thickness measurements of the chemical and biological layers on Si/SiO_2 chips measured using spectroscopic ellipsometry.

S6. Example raw and smoothed data, and Lorentzian fits

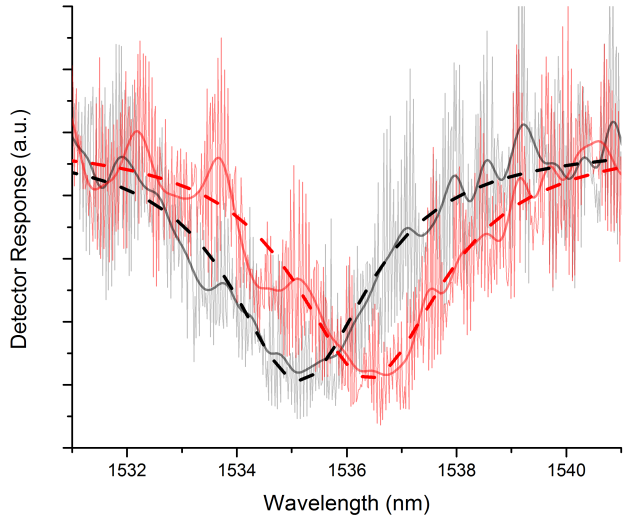

Figure S5: Example optical spectra displaying transmission dip at 21 °C (black) and 37 °C (red), including raw measured spectra ($\Delta\lambda$=0.02 nm) as well as after applying a low-pass filter (solid dark line, 10-point FFT smoother, OriginLab), and a Lorentzian fit (dashed line, OriginLab).

S7. 2D PhC detection of particles under flow (electrostatic capture)

For comparison with the recognition-mediated particle detection experiment, amine-functionalized 280-nm latex particles (in distilled, de-ionized water) were flowed through a microfluidic channel secured above a piranha-cleaned, unfunctionalized 2D PhC sensor (identical in geometry to that used to acquire data shown in Figure 5). In the results shown below, data points indicate the measured resonant wavelength at specific time points. The error bars correspond to the error in fitting a Lorentzian function to the optical transmission spectra. The initial five data points correspond to the baseline resonance measurements of the PhC with water as the cover medium. After flowing the particle suspension at various flow rates, water was flowed over the PhC, represented by last seven scans. As expected, electrostatic interaction between the sensor surface (net negative charge) and the positively charged amine-functionalized particles led to nonspecific, reversible particle capture evidenced by changes in resonance frequency.

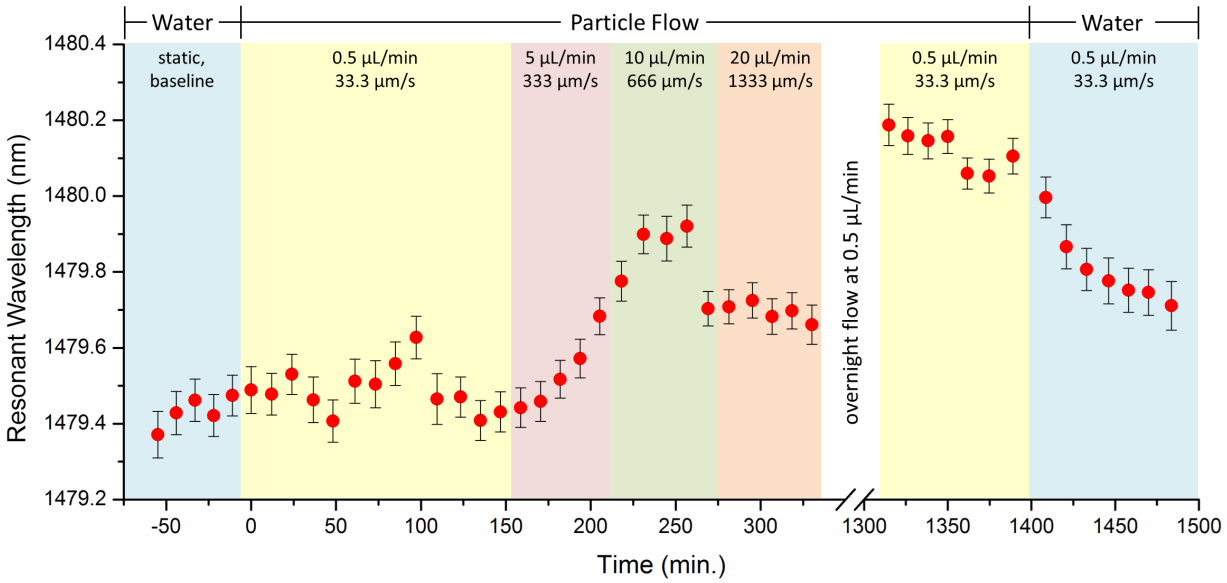

Figure S6: Detection of amine-terminated latex particles (280 nm diameter, in water) with an unfunctionalized PhC sensor under various microfluidic flow rates. Error bars indicate the error of the Lorentzian function fit to the dip in each individual transmission spectrum.

References

1. J. D. Joannopoulos, S. Johnson, J. N. Winn, R. D. Meade, *Photonic crystals: molding the flow of light* (Princeton University Press, Princeton, NJ, ed. 2, 2008), pp. 18.

2. G. Cocorullo and I. Rendina, *Electron. Lett.*, 1992, 28, 83.